High-temperature ferromagnetism by means of oriented nanocolumns: Co clustering in (Zn,Co)O

N. Jedrecy,* H. J. von Bardeleben, and D. Demaille
Institut des Nano Sciences de Paris, Université Pierre et Marie Curie-Paris 6 and CNRS-UMR 7588, 140 rue de Lourmel, 75015 Paris, France

(Received 26 May 2009; revised manuscript received 12 October 2009; published 19 November 2009)

In order to provide insight into the magnetic properties of semiconductors with ferromagnetic inclusions, we present a thorough quantitative analysis of (Zn,Co)O films with high Co concentration, which give rise to high saturation magnetization values ($\sim$110 kA m^{-1}) at room temperature. From the orientation-, temperature-, and field-dependent responses of the magnetization and of the *Q*-band ferromagnetic resonance modes, we give evidence of two types of nanosized ferromagnetic Co clusters and derive their respective contributions. The first type are spherical with diameters about 5 nm and blocking temperatures T_B about 100 K. The second type are elongated along the surface normal and crystallographically oriented with respect to the ZnO host. Some are nanocolumns about 4 nm wide, whose height may reach up to 60 nm, leading to $T_B \geq 300$ K. These results are confirmed by high-resolution transmission electron microscopy analysis. In addition to provide transition from ferromagnetism to superparamagnetism above 300 K, the nanocolumns lead to strong anisotropic magnetic properties. We believe that they could find applications in spintronic devices.

DOI: 10.1103/PhysRevB.80.205204 PACS number(s): 75.50.Pp, 36.40.Cg, 75.30.Gw, 75.75.+a

I. INTRODUCTION

The search for materials combining ferromagnetic with semiconducting properties has resulted in a considerable amount of research work on the so-called diluted magnetic semiconductors (DMSs), e.g., GaMnAs, GaMnN, ZnCrTe, and ZnCoO. The wide range of critical magnetic ordering temperatures as a function of growth conditions has led to consider a specific class of DMSs, characterized by magnetically active transition metal (TM)-rich nanometer-sized precipitates.[1–4] Extrinsic ferromagnetism by nanoclusters might be relevant for spintronic functionalities such as giant magnetoresistance or magnetization switching by current injection.[1,5–9] However, in granular systems, the coupling between magnetism and transport (including the Coulomb blockade transport regime typical of nanoclusters arrays) remains an open question. For instance, the reasons for the anomalous Hall effect, observed in several DMSs with magnetic clustering,[9–11] have not been established so far.

Recently, self-organized embedded magnetic nanocolumns have been achieved in GeMn.[9] This type of nanostructure, highly anisotropic, leads to interesting magnetic and transport properties,[6,9,12] and could open the route for new electronic device architectures.[13] In this paper, we give evidence for the first time of ferromagnetic Co nanocolumns embedded in ZnO and focus on their distinct contribution to the ferromagnetism with respect to spherical Co nanoparticles. We show that clustering in the form of rods is responsible for pronounced anisotropic responses of the magnetization and of the microwave resonance absorption with respect to magnetic field as well as for increased blocking temperatures.

Robust ferromagnetism in (Zn,Co)O thin films, close to or above room temperature, has been attributed either to Co-rich (Zn,Co)O nanocrystals[14] or to metallic Co (or CoZn) nanoclusters.[15–18] In parallel, several reports have laid emphasis on the fact that, when the films exhibit homogeneous high structural quality, the Co^{2+} dopant ions at Zn^{2+} sites of the wurtzite ZnO structure behave paramagnetic[19,20] or couple antiferromagnetically[19–22] between nearest neighbors. Later, element selective studies have demonstrated that metallic Co atoms aggregated in the form of nanoclusters may be present simultaneously with Co^{2+} ions substituting Zn^{2+} in the ZnO host lattice.[15,23,24]

II. EXPERIMENTS

The $Zn_{1-x}Co_xO(0001)$ epitaxial films, with thicknesses of 200–700 nm and $x=0.3$, were herein grown on *c*-sapphire substrates by pulsed laser deposition (PLD), using typically a substrate temperature T of 350 °C and an O_2 pressure P of 1×10^{-7} Torr. These (T,P) conditions as well as the high Co doping level have been settled as necessary to produce robust saturation magnetization values at or above room temperature.[15,23,25] Transmission electron diffraction (TED) measurements have shown that the films have their *c* axis along the surface normal with two possible orientations of the crystalline grains in the plane of the film, rotated from each other by 30°. Magnetic properties were investigated by ferromagnetic resonance (FMR) spectroscopy using either a *X*-band (9.5 GHz) or a *Q*-band (34 GHz) spectrometer as well as by conventional magnetometry using a superconducting quantum interference device (SQUID), at temperatures ranging from 4 to 640 K and in a range of magnetic fields $\mu_0 H$ between 0 and 20 000 G, the angle θ of H with respect to the surface normal being varied from 0° to 90°.

III. MAGNETIZATION MEASUREMENTS

Figure 1(a) shows the H-field dependence of the magnetization M at 5 K, for $\theta=0°$ (squares) and for $\theta=90°$ (triangles). The large saturation magnetization value M_s (126 kA m^{-1}) is roughly the same in the two configurations. On the other hand, a widely open hysteresis M-H loop is observed at 5 K for $\theta=0°$ (out-of-plane magnetic field), comparatively to that for $\theta=90°$ (in-plane field), suggesting an

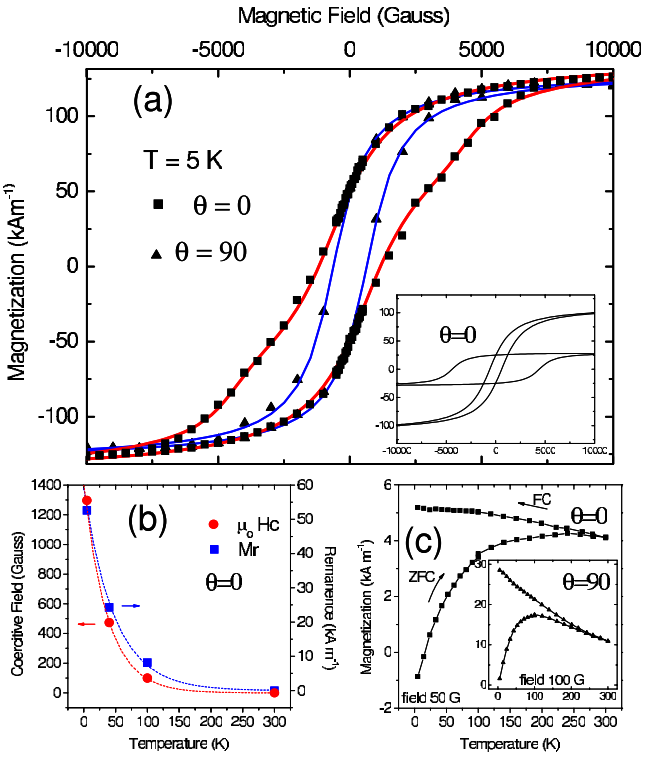

FIG. 1. (Color online) (a) M-H data of the $Zn_{0.7}Co_{0.3}O$ sample at 5 K in the out-of-plane ($\theta=0°$, squares) and in the in-plane ($\theta=90°$, triangles) geometry with their best fit (full lines). The decomposition of the $\theta=0°$ M-H loop is shown in the inset. (b) Coercitive field (left scale) and remanent magnetization (right scale) as a function of temperature for $\theta=0°$. (c) ZFC and FC magnetizations as a function of temperature for $\theta=0°$, with an applied field of 50 G. The same for $\theta=90°$ is shown in the inset.

easy axis along c ZnO. The coercitive field $\mu_0 H_c$ ($\mu_0 H_c = 1300$ G at 5 K) and the remanence M_r ($M_r = 0.42\ M_S$ at 5 K) follow an exponential-like decay as a function of temperature T [see Fig. 1(b)]. This behavior is expected from superparamagnetic clusters, blocked at low temperature. Indeed, the M-H data measured at 300 K (not shown here) may be nicely fitted using the Langevin function L and a giant moment of the clusters equal to $m=8500\ \mu_B$. Assuming metallic Co clusters (1.6 μ_B per atom) of spherical shapes with bulk-like hcp structure, this leads to an average particle diameter $d=5$ nm.

An interesting characteristic of the hysteresis loop at 5 K for $\theta=0°$ is the change in curvature of the lower (upper) branch at about +(−)3000 G. To account for the whole M-H dependence, one has to consider two hysteresis components: one square-like loop with a high coercitive field H_c in the 4000 G range and one tightened S-shaped loop with a reduced remanence/saturation ratio. The best $\theta=0°$ M-H fit is shown as solid lines in Fig. 1(a) (see also the decomposition in the inset). By considering how the two loops composing the $\theta=0°$ M-H signal evolve as a function of T, we could determine that the S-shaped loop component closes at ~100 K. We attribute the origin of the two loops to two different populations of clusters, with two different blocking temperatures, namely, $T_{B1} \sim 100$ K (disappearance of the S loop) and $T_{B2} \sim 300$ K (disappearance of the square loop).

Additional zero-field-cooled (ZFC) and field-cooled (FC) measurements of the magnetization as a function of temperature are shown in Fig. 1(c). The ZFC curve in the $\theta=0°$ geometry shows a large maximum centered about 250 K with an inflexion in the ascending slope at about 100 K. For $\theta=90°$, the ZFC curve shows a pronounced maximum at 100 K, as if this geometry was solely sensible to the first population of clusters. As a matter of fact, the M-H opened loop for $\theta=90°$ and 5 K [Fig. 1(a)] has a single component and closes itself at $T_{B1} \sim 100$ K. These observations lead to envisage an average in-plane size d_1 for all clusters. Using as a criterion (i) $T_{Bi}=KV_i/25$ k where K is the uniaxial magnetocrystalline anisotropy energy density of bulk Co ($K=4.5 \times 10^5$ J m^{-3}) and V_i is the cluster volume (assumed as spherical), one derives from T_{B1} a typical diameter $d_1 = 5.3$ nm. This value is consistent with the value deduced from M-H curves at 300 K (see discussion above). The higher T_{B2} blocking temperature observed in the $\theta=0°$ geometry shows some clusters are ellipsoidal, with the long axis in the out-of-plane direction. With the same criterion (i), if one considers an isotropic size d_1 in the plane of the film, T_{B2} would correspond to clusters with an average height $h_2 = 11$ nm. The elongated shapes along the ZnO c axis, probably driven by the low-temperature growth, suggest c oriented Co clusters, since both ZnO and Co crystallize in hexagonal-type structures.

It is important to note that all dopant Co atoms are not under metallic form. Optical absorption spectroscopy reveals that a significant fraction is instead in Co^{2+}_{Zn} form (substituting Zn^{2+} ions).[15] Defining the volumetric fraction of metallic Co as $f=V_{Co}/V_{film}$, where V_{Co} is the total volume of metallic Co and V_{film} is the film volume, one derives from $M_s=fM$, where M is the bulk Co magnetization, $f=8\%$ ($M_s = 110$ kA m^{-1} at 300 K). A rapid calculation based on the structural parameters of bulk cobalt and ZnO shows that $f = 8\%$ corresponds to an atomic fraction of metallic Co equal to 0.14. This means that for a 30% concentration of Co in ZnO, 14% are metallic and 16% are ionic.

IV. TRANSMISSION ELECTRON MICROSCOPY RESULTS

High-resolution transmission electron microscopy (HRTEM) cross-section images are displayed in Fig. 2. Different types of precipitates, from spherical to columnar, may be identified [Fig. 2(a)–2(c)] thanks to the Moiré fringes produced by the superposition of planes of ZnO and planes of the precipitates. Most Moiré fringes are exactly parallel to the $(0001)_{ZnO}$ planes of ZnO and equidistant with an interfrange $D=9.3 \pm 1.1$ Å. This is the value expected for (0001) planes of hcp bulk Co, parallel to $(0001)_{ZnO}$ (note the latter are distant by $c/2$ in the images). In the direction perpendicular to the c axis (that is $\langle 110 \rangle_{ZnO}$ as derived from TED), one may observe [Fig. 2(b)] other fringes with a spacing of ~5.5 Å. This is indeed expected for aligned $(11\bar{2}0)$ planes (note the $(11\bar{2}0)_{ZnO}$ planes are not visualized because their 1.62 Å interplanar distance is lower than the 1.8 Å microscope resolution). Other types of Moiré may be revealed but analysis of several images shows that clusters mostly adopt the same crystallographic orientation than ZnO. In the plane

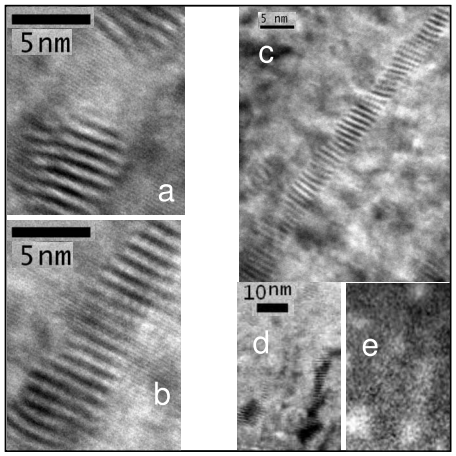

FIG. 2. (a)–(c) HRTEM images showing different types of clusters (spherical, elongated, and columnar) visualized by the help of the Moiré fringes. (d) and (e) TEM and EFTEM at the $L_{2,3}$ Co edge [images rotated by −26° with respect to (a)–(c)].

of the film, the width of the clusters whatever their shape is about 4–5 nm while in the surface normal direction the height may vary from 4 to 60 nm. Nanoscale chemical analysis using electron energy-loss spectroscopy (EELS) at the Co $L_{2,3}$ edge enabled us to identify the distribution of all types of Co clusters [see image 2(d) and the corresponding energy-filtered image 2(e)]. We could observe that clusters with anisotropic shape are always (0001)-oriented (within ±6°) and that the cluster density is significantly higher in the interface region. We recall here that a non negligible proportion of Co atoms are also incorporated as cations in the ZnO lattice,[15] attenuating the contrast of metallic clusters with respect to their surrounding in the EELS mapping. The HRTEM observations fully confirm the SQUID-derived in-plane size of the clusters (which determines T_{B1}), as well as the expansion and dispersion of the out-of-plane size (responsible for the enlarged T_{B2} blocking temperature).

V. FERROMAGNETIC RESONANCE

A. Model

A quantitative analysis of the different terms intervening in the energy of the system (shape anisotropy and magnetocrystalline anisotropy) is made possible by using the angular-dependent dynamic FMR technique. Typical Q-band spectra recorded at room temperature are shown in Fig. 3(a) for two orientation angles θ of the magnetic field. In order to interpret the results, we briefly review some basics of FMR. In an external magnetic field $\mu_0\mathbf{H}$, any magnetization vector $\mathbf{M}$ will precess around the field axis. The magnetic resonance (which corresponds to the microwaves absorption, recorded here as its first derivative) is expected at values of H given by:[26]

$$\left(\frac{h\nu}{g\mu_B}\right)^2 = (\omega/\gamma)^2 = \frac{1}{M_{yz}^2}\left[\frac{\partial^2 E}{\partial\phi^2}\frac{\partial^2 E}{\partial\alpha^2} - \left(\frac{\partial^2 E}{\partial\phi\,\partial\alpha}\right)^2\right]_{eq} \quad (1)$$

where $\nu=\omega/(2\pi)$ is the microwave frequency, g is the spectroscopic splitting factor, E is the free energy density of the system, angles α and ϕ determine the orientation of M, and the label "eq" is used for equilibrium state. Dealing with a heterogeneous film made of ferromagnetic clusters (assumed as single-domain with magnetization $\mathbf{M}$) embedded in a nonmagnetic matrix, we start with three main contributions to E at room temperature:[27]

$$E = -\mathbf{M}\mu_0\mathbf{H} + 1/2\,\mu_0\mathbf{M}N^f f\mathbf{M} + 1/2\,\mu_0\mathbf{M}N^c(1-f)\mathbf{M}, \quad (2)$$

where f is the volumetric fraction of clusters with respect to film (see Sec. III), $N^f=\{0,0,1\}$ and $N^c=\{\varepsilon,\varepsilon,1-2\varepsilon\}$ are the diagonal demagnetizing tensors of the film and of the cluster, respectively. The first term in Eq. (2) represents the Zeeman energy. The second and third term represent the demagnetizing energy due to the thin film shape anisotropy and that due to the cluster shape anisotropy, respectively. It is assumed that the demagnetizing energy is a linear combination of the limiting cases of an isolated cluster ($f=0$) and of a homogeneously magnetized thin film ($f=1$). If uniaxial magnetocrystalline anisotropy intervenes, a fourth supplementary energy term $E'=K_{eff}\sin^2\Psi$, where Ψ is the angle of $\mathbf{M}$ with respect to the easy-magnetization axis, has to be added in Eq. (2). At equilibrium, Eqs. (1) and (2) provide for given values of θ, M, f, ε, two equations that allow us deriving the resonance values of H and ϕ:

$$H\sin(\phi-\theta) = \tfrac{1}{2}M_{eff}\sin(2\phi),$$

$$H_0^2 = [H\cos(\phi-\theta) - M_{eff}\cos^2(\phi)][H\cos(\phi-\theta) - M_{eff}\cos(2\phi)], \quad (3)$$

where $\mu_0 H_0=\omega/\gamma$ (herein ~11 100 G using $\nu=34$ GHz) is the virtual resonance field without magnetization, and

$$M_{eff} = M[1+3\varepsilon(f-1)] - 2K_{eff}/(\mu_0 M), \quad (4)$$

is the effective magnetization of the film in the most general case.

B. FMR results

As shown by Fig. 3(a) the spectra reveal essentially two components C1 and C2, the main one C1 shifting toward high fields by ~1300 G from $\theta=90°$ to $\theta=0°$, the second one C2 shifting toward low fields by ~8900 G. Most spectra may be fitted perfectly on the sole basis of two symmetric Lorentzian lines, except close to $\theta=0°$, where a third component C3 must be considered. The angular dependences of the resonance fields $\mu_0 H_{ri}$ associated to Ci ($i=1,2,3$) derived from fits to experimental spectra are displayed in Fig. 3(b) in reverse scale. We focus our discussion on C1 and C2, which provide the extreme values of the resonance fields that need to be taken into account in our system. As it will appear in the following, C3 is more likely an artifact due to the nonsymmetric distribution of cluster sizes and orientations with respect to the c axis.

The angular variation for C1 is typical of a granular thin film that is a heterogeneous film consisting of magnetic spherical clusters embedded in a nonmagnetic matrix. Indeed, for an isotropic particle shape, the tensor demagnetiz-

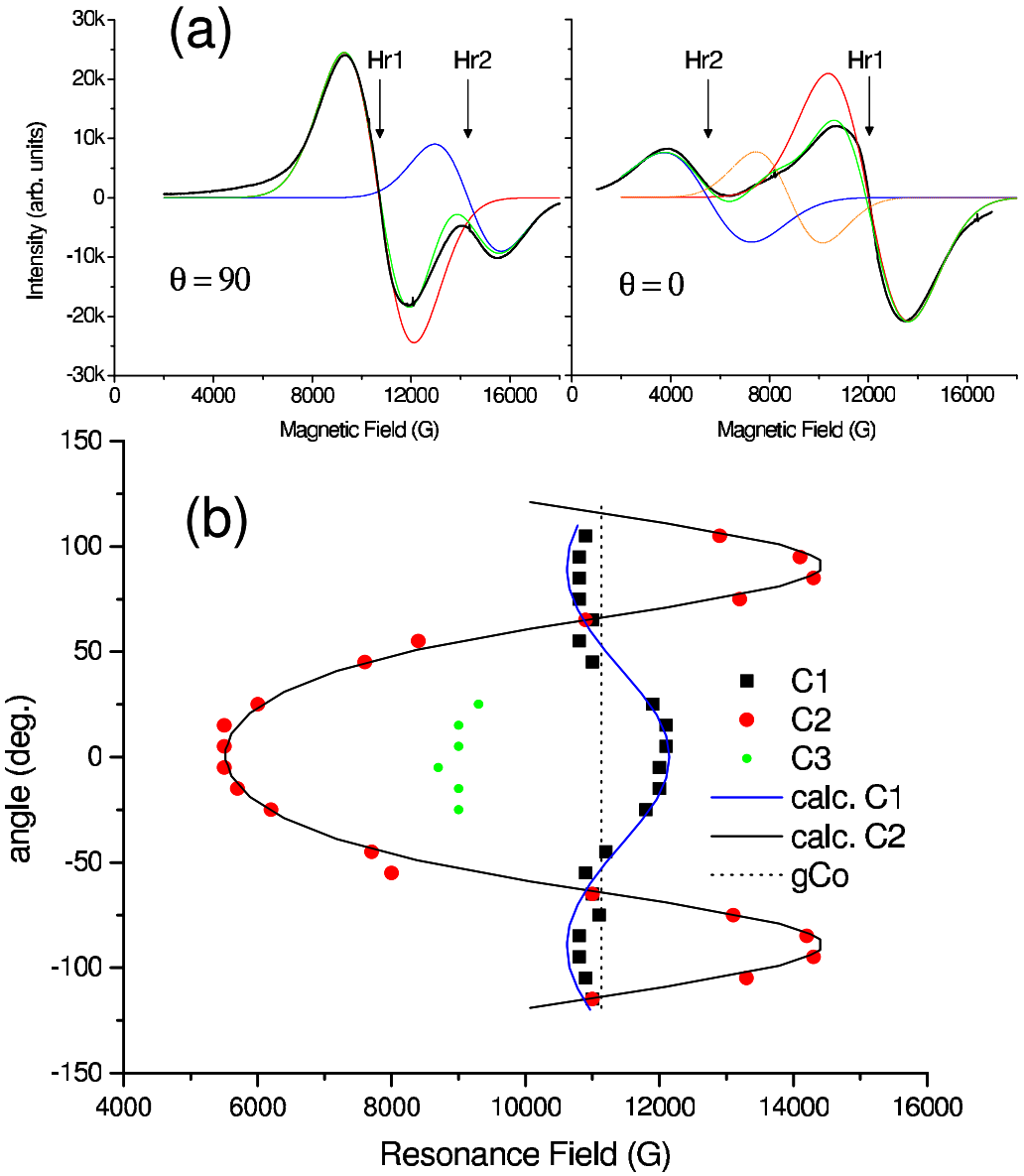

FIG. 3. (Color online) (a) Experimental Q-band FMR spectra (bold lines) at 300 K for angles θ=90° and θ=0°, with their respective decomposition. In addition to the main component C1, a second contribution C2 is seen at higher fields for θ=90° and at lower fields for θ=0°. A third component C3 is needed to achieve a perfect fit of the data for θ=0°. (b) The resonance positions of C1, C2, and C3 as a function of angle θ in X-Y reverse scale with the best simulation (full lines, see text). The resonance position of metal Co atoms is indicated by the vertical dashed line.

ing coefficient is $\varepsilon=1/3$ and the corresponding demagnetizing energy term $1/2\mu_0\mathbf{M}N^c(1-f)\mathbf{M}$ does not depend on α nor ϕ. As a consequence, for $\theta=0$, the resonance field $\mu_0 H_{r1}$ [see Eq. (3)] is displaced toward high fields by an amount $\mu_0 M_{eff}$ with respect to $\mu_0 H_0$, where $M_{eff}=fM$ [or $M_{eff}=fM-2K_{eff}/(\mu_0 M)$]. For $\theta=\pi/2$, $\mu_0 H_{r1}$ is displaced toward low fields according to $(H_0)^2=[H_{r1}+M_{eff}]H_{r1}$. The full experimental shift $\mu_0\Delta H_{r1}$ from θ=90° to θ=0° allows one to evaluate $\mu_0 M_{eff}$=875 G independently of H_0 (and hence of g) since $\Delta H_{r1}\sim 3/2\ M_{eff}$. The g factor consistent with experimental H_{r1} positions is that of bulk Co: g=2.18. The calculated curve $\mu_0 H_{r1}$ as a function of θ is displayed as a solid line in Fig. 3(b). It is worthwhile to mention that the dominant contribution C1 at Q band follows the same angular dependence than that observed at X band, except $\mu_0 H_0$ =3100 G in this latter case (ν=9.5 GHz).

The C2 signal, whose intensity is about the third of the C1 signal [Fig. 3(a)] behaves as highly anisotropic and must be attributed to the presence of nonspherical clusters. A remarkable feature directly apparent from Fig. 3(b) is that the H_{r2}-θ dependence is exactly of inverse curvature with respect to H_{r1}-θ. Since the shift of the C1 signal from $\mu_0 H_0$ toward higher field is mainly due to the demagnetizing field induced by the thin film geometry ($-N^f fM=-fM_z$, where z refers to the reduced dimension), the inverse behavior of the C2 spectrum reveals the presence of a demagnetizing field in the plane of the film, that is a columnar geometry. As a matter of fact, infinite cylinders with the long axis parallel to z (in this

model hypothesis, the related tensor demagnetizing coefficient is $\varepsilon=0.5$), yield an angular dependence close to that observed for C2, although of higher magnitude. The two $\mu_0 H_{r2}$ values at $\theta=90°$ and $\theta=0°$ derived from Eq. (3) using $f=8\%$ are in this case ($\varepsilon=0.5$) 14900 and 4520 G, respectively.

C. Discussion

If one neglects crystalline anisotropy, setting magnetization M to the value of bulk Co ($\mu_0 M=17\,500$ G), one derives from the magnitude of M_{eff} a volumetric fraction $f=5\%$. This is at variance with SQUID measurements at 10 000 G and at 300 K which provide the value $f=8\%$ ($M_s=110$ kA m^{-1}, $\mu_0 M_s=\mu_0 fM=1380$ G). Therefore, crystalline anisotropy contributes at 300 K for an amount $2K_{\text{eff}}/M=525$ G and *in fine* $M_{\text{eff}}=fM-2K_{\text{eff}}/\mu_0 M$ with $f=8\%$ in agreement with SQUID results (notice the crystalline anisotropy field for a bulk Co crystal is $2K/M=6465$ G). The exact experimental H_{r2}-θ dependence [see Fig. 3(b)] can be nicely simulated setting f and K_{eff} to the above values, and considering anisotropic cluster shapes characterized by a demagnetizing coefficient $\varepsilon=0.47$ instead of 0.5.

In conclusion, the excited FMR C1 and C2 modes appear as the individual responses of Co clusters, spherical, or largely elongated along the surface normal direction, respectively. This corroborates the previous assumption derived from SQUID magnetometry of two types of clusters with respective blocking temperatures $T_{B1}=100$ K (spherical nanoclusters) and $T_{B2}=300$ K (columnar nanoclusters). On the basis of the FMR C1 and C2 signal intensities, the volumetric fractions of clusters 1 and 2 are $f_1=6\%$ and $f_2=2\%$, respectively, ($f=f_1+f_2$). These values agree with the saturation values of each M-H component for $\theta=0°$.

Our modeling assumes given shapes of clusters, namely perfectly spherical, or columnar with a characteristic coefficient $\varepsilon=0.47$. It provides the two H_{ri}-θ variations ($i=1,2$) associated to the two main experimental resonance peaks. Actually, each of the latter is an average of the contributions of either spherical clusters with a diameter d_1 distribution or columnar clusters with a height/width distribution (and hence a distribution of ε values). Those distributions are most probably non symmetric, whereas we have considered symmetric Lorentzian line shapes. Hence, it is expected that some experimental features (in particular, the FMR contribution at $\theta=0°$ close to 9000 G) are not perfectly reproduced restricting ourselves to two components. The C3 component may indeed be explained by clusters characterized by $\varepsilon=0.41$ (in this case, $H_{r3}=8800$ G at $\theta=0°$) a value in between 1/3 and 1/2. A more rigorous treatment (out of the scope of this paper) would involve considering an asymmetric line shape, as the result of an asymmetric ε distribution.

Other observations could be made, some of which are briefly reported in the following. We could perform the measurement of the *X*-band FMR signal (not shown here) from 4 to 640 K. The *X*-band signal is largely asymmetric in the 4–350 K temperature range, and the resonance position shifts from low fields as a function of raising temperature, while the signal width decreases. Thermal fluctuations are known to induce the narrowing of a superparamagnetic resonance spectrum; the peak displacement suggests that at low temperature magnetocrystalline energy terms more intervene in the equilibrium process. From 350 to 640 K, the signal becomes more and more symmetric while its position does not change anymore. This is consistent with the fact that, above 300 K (T_{B2}), thermal fluctuations begin to overpass the magnetocrystalline and shape anisotropy energy barriers of most of the clusters.

Although the *M-H* loop for $\theta=0°$ closes itself at about 300 K, the saturation magnetization $M_s=fM$ keeps a significant value well above this temperature. Extrapolation of our M_s data as a function of T, according to Bloch's law, points toward a critical Curie temperature $T_c\sim 1250$ K, consistent with that of bulk cobalt. We could verify *a posteriori* by *Q*-band FMR and SQUID that annealing at 640 K negligibly affects the Co distribution in the film. Lastly, no shift of the magnetization loop *M-H* could be observed after cooling in a 50 000 G field, thus excluding the presence of antiferromagnetic CoO shells surrounding the Co clusters.

VI. CONCLUSION

In conclusion, we have revealed the formation of crystallographically oriented Co nanocolumns in ZnCoO films with high Co concentration, leading to strong anisotropic ferromagnetic signatures up to temperatures close to 300 K. This result may be important in the context of current search for magnetic semiconductors aimed at constituting one electrode of a magnetic tunnel junction or a spin injector (one may use the nanocolumns as current channeling paths). Our work also demonstrates the sensitivity of the noninvasive FMR technique to magnetic nanoinclusions and importantly how it may unambiguously discriminate between different shapes and orientations.

ACKNOWLEDGMENTS

We are indebted to our colleagues of the Thales group in Orsay (J.-P. Contour, A. Anane, and A. Fert) for providing us with the samples used in this study. We thank J. Siejka (INSP) for RBS results and M. Cubukcu for assistance during SQUID operations. We acknowledge support from Region Ile-de-France to the cryoelectron microscope JEOL 2100F installed at IMPMC and wish to thank B. Capelle.

*jedrecy@insp.jussieu.fr

[1] S. Kuroda, N. Nishizawa, K. Takita, M. Mitome, Y. Bando, K. Osuch, and T. Dietl, Nat. Mater. **6**, 440 (2007).
[2] M. Yokoyama, H. Yamaguchi, T. Ogawa, and M. Tanaka, J. Appl. Phys. **97** 10D317 (2005).
[3] X. Y. Cui, B. Delley, A. J. Freeman, and C. Stampfl, Phys. Rev. B **76**, 045201 (2007).
[4] D. Bougeard, S. Ahlers, A. Trampert, N. Sircar, and G. Abstreiter, Phys. Rev. Lett. **97**, 237202 (2006).
[5] P. Hai, S. Ohya, M. Tanaka, S. E. Barnes, and S. Maekawa, Nature (London) **458**, 489 (2009).
[6] A. P. Li, C. Zeng, K. van Benthem, M. F. Chisholm, J. Shen, S. V. S. Nageswara Rao, S. K. Dixit, L. C. Feldman, A. G. Petukhov, M. Foygel, and H. H. Weitering, Phys. Rev. B **75**, 201201(R) (2007).
[7] R. P. Tan, J. Carrey, C. Desvaux, L.-M. Lacroix, P. Renaud, B. Chaudret, and M. Respaud, Phys. Rev. B **79**, 174428 (2009).
[8] O. Riss, A. Gerber, I. Ya. Korenblit, A. Suslov, M. Passacantando, and L. Ottaviano, Phys. Rev. B **79**, 241202(R) (2009).
[9] M. Jamet, A. Barski, T. Devillers, V. Poydenot, R. Dujardin, P. Bayle-Guillemaud, J. Rothman, E. Bellet-Almaric, A. Marty, J. Cibert, R. Mattana, and S. Tatarenko, Nat. Mater. **5**, 653 (2006).
[10] S. R. Shinde, S. B. Ogale, J. S. Higgins, H. Zheng, A. J. Millis, V. N. Kulkarni, R. Ramesh, R. L. Greene, and T. Venkatesan, Phys. Rev. Lett. **92**, 166601 (2004).
[11] M. Snure, D. Kumar, and A. Tiwari, Appl. Phys. Lett. **94**, 012510 (2009).
[12] S. Caprara, V. N. Men'shov, V. V. Tugushev, P. M. Echenique, and E. V. Chulkov, Phys. Rev. B **79**, 035202 (2009).
[13] T. Yang, T. Kimura, and Y. Otani, Nat. Phys. **4**, 851 (2008).
[14] T. Dietl, T. Andrearczyk, A. Lipinska, M. Kiecana, M. Tay, and Y. Wu, Phys. Rev. B **76**, 155312 (2007).
[15] H. J. von Bardeleben, N. Jedrecy, and J.-L. Cantin, Appl. Phys. Lett. **93**, 142505 (2008).
[16] T. C. Kaspar, T. Droubay, S. M. Heald, M. H. Engelhard, P. Nachimuthu, and S. A. Chambers, Phys. Rev. B **77**, 201303(R) (2008).
[17] D. P. Norton, M. E. Overberg, S. J. Pearton, K. Pruessner, J. D. Budai, L. A. Boatner, M. F. Chisholm, J. S. Lee, Z. G. Khim, Y. D. Park, and R. G. Wilson, Appl. Phys. Lett. **83**, 5488 (2003).
[18] S. M. Heald, T. Kaspar, T. Droubay, V. Shutthanandan, S. Chambers, A. Mokhtari, A. J. Behan, H. J. Blythe, J. R. Neal, A. M. Fox, and G. A. Gehring, Phys. Rev. B **79**, 075202 (2009).
[19] N. Jedrecy, J. von Bardeleben, Y. Zheng, and J.-L. Cantin, Phys. Rev. B **69**, 041308(R) (2004).
[20] A. Ney, K. Ollefs, S. Ye, T. Kammermeier, V. Ney, T. C. Kaspar, S. A. Chambers, F. Wilhelm, and A. Rogalev, Phys. Rev. Lett. **100**, 157201 (2008).
[21] M. Kobayashi, Y. Ishida, J. I. Hwang, T. Mizokawa, A. Fujimori, A. K. Mamiya, J. Okamoto, Y. Takeda, T. Okane, Y. Saitoh, Y. Muramatsu, A. Tanaka, H. Saeki, H. Tabata, and T. Kawai, Phys. Rev. B **72**, 201201(R) (2005).
[22] M. Bouloudenine, N. Viart, S. Colis, J. Kortus, and A. Dinia, Appl. Phys. Lett. **87**, 052501 (2005).
[23] K. Rode, R. Mattana, A. Anane, V. Cros, E. Jacquet, J.-P. Contour, F. Petroff, A. Fert, M.-A. Arrio, Ph. Sainctavit, P. Bencok, F. Wilhelm, N. B. Brookes, and A. Rogalev, Appl. Phys. Lett. **92**, 012509 (2008).
[24] K. Potzger, K. Kuepper, Q. Xu, S. Zhou, H. Schmidt, M. Helm, and J. Fassbender, J. Appl. Phys. **104**, 023510 (2008).
[25] K. Rode, A. Anane, R. Mattana, J.-P. Contour, O. Durand, and R. LeBourgeois, J. Appl. Phys. **93**, 7676 (2003).
[26] J. Smit and H. G. Beljers, Philips Res. Rep. **10**, 113 (1955).
[27] U. Netzelmann, J. Appl. Phys. **68**, 1800 (1990).